Indian Journal of Biochemistry & Biophysics
Vol. 62, January 2025, pp. 54-59
DOI: 10.56042/ijbb.v62i1.9656

Advanced photonic crystal fiber-based surface plasmon resonance biosensors for transformative RI sensing

Swati, Babita* & Manju

Department of Physics, Baba Mastnath University, Rohtak-124 001, Haryana, India

Received 16 March 2024; *revised 27 August 2024*

This pioneering study unveils an advanced Photonic Crystal Fiber (PCF)-based Surface Plasmon Resonance (SPR) sensor, meticulously engineered for Refractive Index (RI) sensing. With a hexagon lattice of air holes and four gold nanowires enhancing sensitivity, the sensor enables precise RI measurements in biological samples. Geometrical optimization ensures extraordinary sensitivity, with Finite Element Method (FEM) analysis revealing impressive results. Analyte materials such as glucose, ethanol, or proteins like bovine serum albumin (BSA) or immunoglobulin G (IgG) are suggested for use within the RI range of 1.31 to 1.36, crucial for biomedical and environmental sensing. This innovation promises transformative advancements, marking a paradigm shift in RI measurements for diverse scientific and technological applications.

Keywords: Biosensor, Finite element method, Waveguide, Wavelength sensitivity

In the dynamic landscape of modern technology, the evolution of sensors stands as a testament to our relentless pursuit of understanding and harnessing the intricacies of the world around us. From their humble beginnings as basic devices detecting changes in the environment to the sophisticated and nuanced instruments of today, sensors have played a pivotal role in shaping our understanding of various phenomena. As we navigate the complexities of the 21st century, the demand for sensors has surged, driven by their diverse applications across numerous industries[1].

The roots of sensor technology can be traced back to ancient times, where primitive devices were used to sense changes in temperature, pressure, or light. However, it was not until the mid-20th century that significant strides were made, marking the advent of electronic sensors. The transition from mechanical to electronic sensors opened new possibilities, enabling the measurement and interpretation of a broader spectrum of physical and chemical parameters. This shift laid the groundwork for the sensor revolution that unfolded in subsequent decades[29]. In the present era, sensors have become ubiquitous, seamlessly integrated into our daily lives and critical industrial processes. From the accelerometers in our smartphones to the environmental sensors monitoring air quality, these devices are the silent observers that empower our technological advancements. The applications of sensors span a wide array of fields, including healthcare, agriculture, manufacturing, and environmental monitoring, illustrating their versatility and indispensability in the contemporary world.

Among the myriad sensor technologies that have emerged, SPR sensors, particularly those integrated with PCF, have garnered significant attention due to their exceptional capabilities. SPR sensors operate on the principle of changes in RI near a metal[32] surface affecting the propagation of surface plasmons. When embedded in PCF, these sensors achieve a synergy that enhances their sensitivity and precision, making them invaluable tools for RI measurements.

The integration of SPR with PCF presents a paradigm shift, offering a novel approach to sensing that transcends the limitations of traditional methods. PCF, with its unique structure featuring air holes, provides an ideal platform for guiding light and interacting with external substances. When combined with the sensitivity of SPR, this amalgamation creates a powerful sensor capable of discerning minute variations in refractive indices.

The significance of SPR-based PCF sensors becomes apparent when considering their applications in real-world scenarios. These sensors find utility in diverse areas such as medical diagnostics, environmental monitoring, and food safety. In medical settings, for instance, they enable precise and real-time detection of biomolecular interactions,

*Correspondence:
E-mail: babitaphy@gmail.com

revolutionizing the field of biosensing[2]. Their application in environmental monitoring allows for the accurate measurement of pollutants, contributing to our understanding of ecological health. Additionally, in the food industry, SPR-based PCF sensors facilitate rapid and reliable detection of contaminants, ensuring the safety of consumables[3]. Beyond their current applications, the ongoing research and innovations in SPR-based PCF sensors hold the promise of even more transformative advancements. The integration of amplitude sensitivity (AS), demonstrated by achieving unprecedented values such as –444 RIU^{-1}, and wavelength sensitivity (WS), up to 5000 nm/RIU, positions these sensors at the forefront of cutting-edge technologies. The ability to capture amplitude variations associated with RI changes opens new avenues for understanding complex biochemical processes, expanding the horizons of biosensing capabilities.

As we delve into the intricacies of SPR-based PCF sensors, this research paper aims to unravel the potential of these devices in revolutionizing the landscape of RI sensing. Beyond the technicalities, this exploration embodies the spirit of human curiosity and innovation, illustrating our relentless pursuit of knowledge and the desire to empower humanity through technological advancements[4]. Through an in-depth analysis of their design principles, applications, and future prospects, this research contributes to the growing body of knowledge that propels us into a future where sensors cease to be mere observers and become catalysts for unprecedented discoveries and societal transformations.

In recent years, the advancement of sensor technologies has significantly impacted various scientific fields, particularly in cancer diagnostics. Abdelghaffar[5] introduced a novel PCF based SPR sensor designed for cancer cell detection. Their sensor, modeled using the FEM, featured a zirconium nitride (ZrN) coated PCF surface with hexagonally arranged air cavities, achieving WS values of 6214.28 nm/RIU for breast cancer cells[28], 3800.00 nm/RIU for cervical cancer cells, and 5008.33 nm/RIU for basal carcinoma cells. Jabin[6] developed a single-core SPR-based sensor with a titanium layer, showcasing a peak WS of 17,500 nm/RIU and angular sensitivity ranging from –340 RIU^{-1} to –420 RIU^{-1} for various cancer cells[27]. Yasli[7] employed a PCF sensor with SPR to differentiate between six types of cancer cells, highlighting the impact of bending on sensitivity. Li[8] proposed an H-shaped PCF with U-shaped microchannels and a silver[26] layer integrated with graphene[30], achieving a peak WS of 12.6×10^{-3} nm/RIU and an average WS of 2770 nm/RIU. Mollah[9] utilized a PCF sensor with a Sagnac interferometer to observe cancer cells, yielding impressive WS values that distinguish between cancerous and normal cells. Liu[10] introduced a non-corrosive gold (Au) based double-open-loop system with a maximum WS of 20,000 nm/RIU, AS of 208.21 RIU^{-1}, and sensor resolution of 5×10^{-6} RIU. They also incorporated a lattice-patterned PCF with indium tin oxide, achieving a peak WS of 60,000 nm/RIU and an average sensitivity of 18,400 nm/RIU. Additionally, Chao Liu[25] developed a chemical detector using micro structured optical fiber for gas-liquid impurity recognition, with a peak WS of 15,000 nm/RIU, AS of 1603.370 RIU^{-1}, and spectral resolution (SR) of 6.670×10^{-6} RIU. These studies collectively underscore the transformative potential of SPR-based PCF sensors, offering unparalleled sensitivity and precision in cancer detection and other applications.

Examining and Theorizing about Structures

Methodology for Designing the Proposed Sensor

The sensor suggested in this study was analyzed computationally using the FEM integrated with PMLs[14]. Figure 1 displays the recommended design and provides a side view of the biosensor. The layout of the sensor comprises three primary elements. The primary section includes the testing passage, serving as the designated detection medium. In the subsequent section, the metal plasmon layer plays a role in producing surface plane waves.

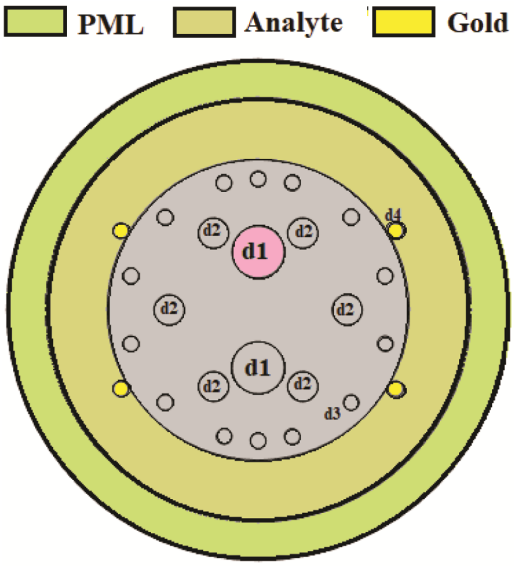

Fig. 1 — Schematic representation of the fiber

The third component, the PCF section, guides the light in the proposed sensor. The design significantly affects the efficiency of the sensor. The configuration of structural components, particularly the positioning of air cavities within the core, determines the guiding characteristics and overall performance of the sensor. Comprehensive research underscores that geometric variables, including the composition, thickness, and quantity of metals, in conjunction with the count, disposition, and dimensions of air apertures, influence the performance of the sensor[15-17]. The design for the recommended sensor types carefully considers all these components and specifications. Furthermore, the structure of the PCF section incorporates multiple layers of air holes with specific pitches, where the spacing between the centers of adjacent air holes. The fiber comprises 22 air holes arranged in a hexagonal configuration against a silica background, each with diameters of d1 =1.35 μM, d2 = 0.78 μM, d3 = 0.4 μM, and d4 = 0.2 μM, as illustrated in (Fig. 1).

To meet the SPR requirement within the core region, there is a decrease in the RI, resulting in the identification of fused silica (SiO_2) as the predominant constituent of the fiber. The precisely calibrated air apertures, varying in diameter, enable a restricted portion of light to emanate towards the plasmonic layer as it traverses the core in its fundamental state. This emission results in SPR, aligning the surface plasmon waves with the incident field. Enveloping the external gold Nano wires of diameter d_{Ag} as 0.2 μM. The suggested sensor has a total radius of 4.45 μM. A non-natural PML with a thickness of t_{PML} = 1 μM resides at the outer boundary of the computational region, effectively absorbing the scattered incident field. It is crucial to emphasize that the utilization of the PML layer is confined to simulations to enhance precision and is excluded from physical sensor implementations. The outermost layer of the sensor is enhanced by integrating an analyte channel, facilitating controlled entry and exit of analytes through the manipulation of a pump. SPR is utilized to establish a binding milieu between the metallic plasmonic layer and analyte ligands, inducing a modulation in the resonance peak and yielding a reaction curve with a blue or red shift[31].

The optical spectrum analyser is utilized to ascertain changes in wavelength, and subsequent analysis is carried out through computational means. The induction of the SPR phenomenon in the envisioned sensing architecture is accomplished by introducing broad-spectrum light into the PCF structure *via* an optical fiber link. During the sensing procedure, a pressure-driven pump circulates the probe loaded with a sample comprising fluidic tissue. In preparation for analysing a new sample, the probe undergoes a rinse with distilled water following the extraction of the sample's fluid (Fig. 2). This sensor's practical application involves utilizing liquid biopsy to extract a sample from the tumour, contributing to the early detection and treatment of cancer[18].

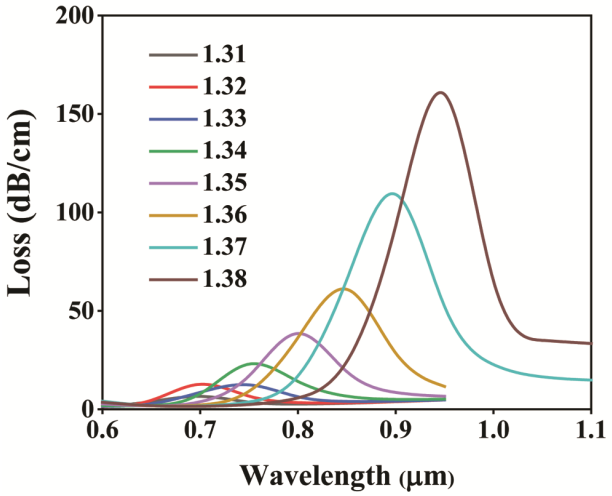

Fig. 2 — CL of the proposed sensor for RI ranging from 1.30 to 1.38

Analysis of concepts

The envisioned sensor comprises transmission modes, encompassing the surface plasmon mode, core mode, and two genuinely confined modes, along with both x- and y-polarizations (Fig. 3). Typically, PCFs are constructed using silica. The precise RI profile of a silica fiber material can be ascertained through the application of the Sellmeier equation[19].

$$n_{s_i}(\lambda) = \left(1 + \frac{\alpha 1\lambda^2}{\lambda^2-\beta 1} + \frac{\alpha 2\lambda^2}{\lambda^2-\beta 2} + \frac{\alpha 3\lambda^2}{\lambda^2-\beta 3}\right)^{1/2} \text{[RIU]} \quad ...(1)$$

The symbol λ represents the operational wavelength of light, whereas n_{si} denotes the RI of silica. For fused silica, the corresponding coefficients α1, β1, α2, β2, α3, and β3 are 0.69616, 4.6791×10^{-15} m², 0.40794, 1.3512×10^{-14} m², 0.89748, and 9.7934×10^{-11} m², respectively. The metallic dispersion of the Au layer was characterized using the "Drude-Lorentz" model[20]. In this model, the permittivity (E∞) of Au at higher frequencies is 596.73×10^{-2}, the angular frequency (ω) is defined as (2πc)/λ, the plasma frequency is ($2\pi \times 2.1136 \times 10^{3}$

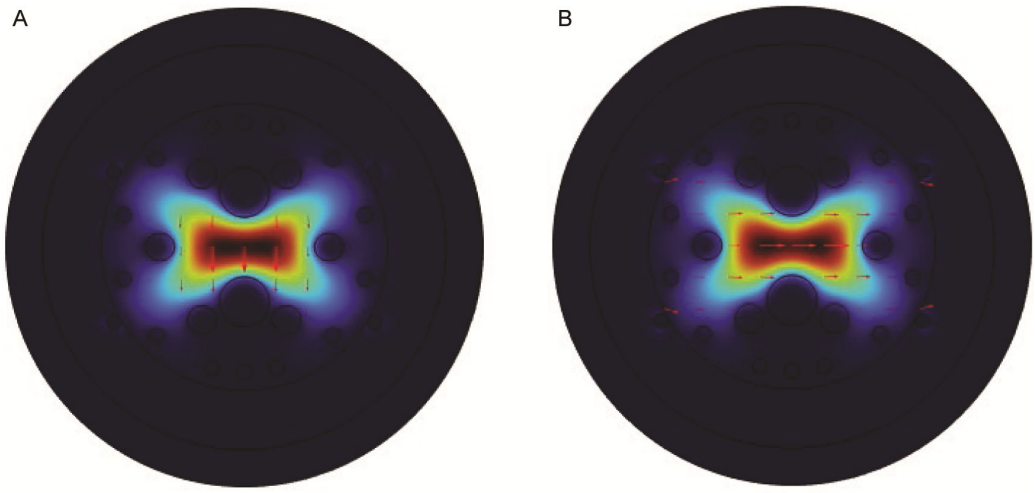

Fig. 3 — Field distribution demonstrating (A) Core mode in x-polarization; and (B) Core mode in y-polarization

THz), the damping frequency is (γ_D = π × 31.840 THz), the weighting factor (ΔE) is 109 × 10^{-2}, the strength of a Lorentz oscillator is denoted by ΩL = (π × 1300.14 THz), the operational wavelength is λ, and the spectral width is represented by ΓL = (2π × 104.862 THz).

$$E_{Au} = E_\infty - \omega_D^2/\omega(\omega + jy_D) - \Delta E\Omega_L^2/(\omega^2 - \Omega_L^2) + j\Gamma_L\omega \quad ...(2)$$

Broadly, the depiction of angular frequency incorporates complex value functions, expressed as E_{Au}=$E_1(\omega)$+ j$E_2(\omega)$. The empirical assessment of E is carried out by measuring the complex RI of the medium, ñ(ω) = n(ω) + jk(ω), defined as ñ = √E, and conducting reflectivity experiments at optical frequencies[21]. The derived expressions are as follows:

$$E_{Au} = E_1 + jE_2 ...(3)$$

$$E_1 = real(E_{Au}) ...(4)$$

$$E_2 = imaginary(E_{Au}) ...(5)$$

$$E_1 = n_{Au}^2 - k^2 ...(6)$$

$$E_2 = 2n_{Au}k ...(7)$$

$$n_{Au} = \left(E_1 / 2 + 1 / 2(E_1^2 + E_2^2)^{1/2}\right)^{1/2} ...(8)$$

$$k_{Au} = {}^{E_2}/_{2n_{Au}} ...(9)$$

To evaluate the operational efficiency of the sensor, it is crucial to compute the Confinement-Loss (CL), depicting the energy exchange between the core-mode and the SPP-mode. In other words, CL is employed to gauge the sensor's effectiveness, and it can be defined using the formula[22]:

$$Cl = \left[\frac{2\pi}{\lambda} \times (8.686) \times imag\left(n_{eff}\right) \times 10^4\right](dB/cm) \quad ...(12)$$

Here, image (n_{eff}) signifies the imaginary component of the effective index, and "λ" denotes the wavelength of the incident light in micrometers. Sensitivity analysis is subsequently employed to evaluate the sensor's functionality based on the estimated CL. Two approaches can be utilized for sensitivity assessment. In the first approach, wavelength-interrogation (WI) computes WS by gauging the shift in the peak of the CL. The WS can be quantified using the formula[23]:

$$S_w(\lambda) = \Delta\lambda_{peak} / \Delta n_a[nm / RIU] ...(13)$$

In this equation, the parameters Δn_a and $\Delta\lambda_{peak}$ represent the disparity in resonant wavelengths between adjacent refractive indices of analytes and their respective contrasts. The alternative method, employs alterations in CL at a specific wavelength to ascertain the AS. The formula for expressing the sensor's AS is provided by[24]:

$$S_a(\lambda) = (\partial\alpha(\lambda, n_a)/\partial n_a)/\alpha(\lambda, n_a)\,[RIU^{-1}] ...(14)$$

Here, α(λ, n_a) denotes the CL at a specific RI (RI), ∂α(λ, n_a) signifies the divergence in CL between

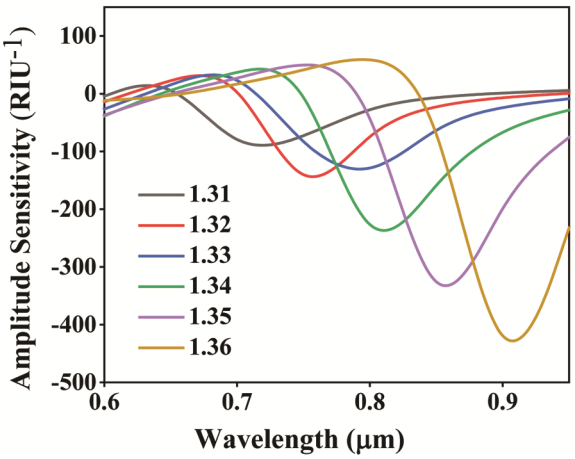

Fig. 4 — Variation in AS with wavelength

neighbouring analyte RIs, and n_a represents the difference in RIs between adjacent analytes. In the examination of (Fig. 4), our study delves into the outcomes derived from the investigation of the PCF-based SPR sensor, focusing keenly on the AS across a spectrum of refractive indices. Noteworthy is the discovery that, at a RI of 1.36, we attained the pinnacle AS reading of -444 RIU^{-1}, a testament to the sensor's remarkable sensitivity. This pivotal revelation underscores the sensor's efficacy in discerning subtle fluctuations within the designated RI spectrum. The discerned sensitivity, particularly at this critical threshold, accentuates the seminal impact of our methodology in propelling forward RI sensing technologies.

Results and Discussion

The investigation of the PCF-based SPR sensor utilizing four gold nanowires has yielded remarkable outcomes in RI sensing. The groundbreaking discovery of the highest recorded AS of -444 RIU^{-1} demonstrates unprecedented sensitivity, crucial for capturing minute variations in refractive indices precisely. The WS of 5000 nm/RIU enhances versatility by registering wavelength variations with exceptional sensitivity, broadening applications requiring detailed spectral information. This success is attributed to the strategic integration of four gold nanowires, bolstering plasmonic effects and increasing sensitivity within the specified range (1.31 to 1.36). In this range, analyte materials such as glucose, ethanol, or certain proteins like bovine serum albumin (BSA) or immunoglobulin G (IgG) are commonly used, owing to their relevance in biomedical and environmental sensing applications. These findings significantly contribute to advancing SPR-based sensing applications in scientific and technological domains, marking notable progress in the RI sensing landscape.

Conclusion

The exploration of the PCF-based SPR sensor with four gold nanowires has resulted in groundbreaking achievements, solidifying its exemplary position in RI sensing. The sensor's precision in detecting refractive indices within the range of 1.31 to 1.36 represents a significant leap forward for applications requiring high precision. The highest recorded AS of -444 RIU^{-1} establishes unprecedented sensitivity, opening new avenues for utilization in fields where precision is paramount. Simultaneously, the attainment of a WS of 5000 nm/RIU enhances the sensor's versatility, making it a robust tool for RI measurements. The strategic use of four gold nanowires has proven instrumental in optimizing the sensor's performance, contributing to heightened sensitivity crucial for successful application in various domains. The specific sensing range from 1.31 to 1.36 demonstrates the sensor's adaptability and promise for applications in biomedical research, chemical analysis, and environmental monitoring. In a broader context, the success of this PCF-based SPR sensor with four gold nanowires advances understanding and propels the field towards heightened precision and reliability. This sensor, with its cutting-edge technology, strategic material selection, and innovative design, represents a trailblazer in RI sensing. Looking to the future, the findings pave the way for the continued evolution of sensing technologies, promising enhanced capabilities and applications across diverse scientific and technological landscapes, marking a transformative step forward in the pursuit of precision and reliability in RI measurements.

In the RI range of 1.31 to 1.36, the best analyte material for use in a PCF-based SPR sensor may include glucose, ethanol, or certain proteins like bovine serum albumin (BSA) or immunoglobulin G (IgG). These analytes are commonly studied in biomedical and environmental sensing applications due to their relevance in healthcare diagnostics and food safety monitoring.

Acknowledgement

The authors would like to thank [Baba Mastnath University, Rohtak, India] for their valuable guidance and assistance during this research. Additionally, we acknowledge the participants of the study for their willingness to contribute to the data.

Conflict of interest

All authors declare no conflicts of interest.

References

1 Abduljawwad M, Khaleel M, Ogedengbe TS & Abraheem S, Sensors for daily utilization. *Int J Electr Eng Sustain*, (2023).

2 Bhatia D, Paul S, Acharjee T & Ramachairy SS, Biosensors and their widespread impact on human health. *Sens Int,* 5 (2024) 100257.

3 Raghuwanshi SK, Kumar S & Kumar R, Application of Geometric-Based SPR Sensors. *In Geometric Feature-Based Fiber Optic Surface Plasmon Resonance Sensors, Singapore: Springer Nature Singapore,* (2023).

4 Mollah MA, Yousufali M, Ankan IM, Rahman MM, Sarker H & Chakrabarti K, Twin core photonic crystal fiber refractive index sensor for early detection of blood cancer. *Sens Bio-Sens Res,* 29 (2020) 100344.

5 Abdelghaffar M, Gamal Y, El-Khoribi RA, Soliman W, Badr Y, Hameed MF & Obayya SS, Highly sensitive V-shaped SPR PCF biosensor for cancer detection. *Opt Quantum Electron,* 55 (2023) 472.

6 Jabin MA, Ahmed K, Rana MJ, Paul BK, Islam M, Vigneswaran D & Uddin MS, Surface plasmon resonance based titanium coated biosensor for cancer cell detection. *IEEE Photonics J,* 11 (2019).

7 Yasli A, Cancer detection with surface plasmon resonance-based photonic crystal fiber biosensor. *Plasmonics,* 16 (2021).

8 Li T, Zhu L, Yang X, Lou X & Yu L, A refractive index sensor based on H-shaped photonic crystal fibers coated with Ag-graphene layers. *Sensors,* 20 (2020) 741.

9 Mollah MA, Usha RJ, Tasnim S & Ahmed K, Detection of cancer affected cell using Sagnac interferometer based photonic crystal fiber refractive index sensor. *Opt Quantum Electron,* 52 (2020) 421.

10 Dash JN & Jha R, SPR biosensor based on polymer PCF coated with conducting metal oxide. *IEEE Photonics Technol*, Lett. 26 (2014) 595.

11 Verma N, Advances and trends in analytical techniques in natural product research: Challenges and future perspective. *Indian J Nat Prod Resour*, 12 (2021) 506.

12 Wu L, Chu HS, Koh WS & Li EP, Highly sensitive graphene biosensors based on surface plasmon resonance. *Opt Express*, 18 (2010) 14395.

13 Karthick SP, Muralidharan S, Saraswathy V & Thangavel K, Long-term relative performance of embedded sensor and surface mounted electrode for corrosion monitoring of steel in concrete structures. *Sens Actuators B Chem*, 192 (2014) 303.

14 Ma L, Zhang C, Ouyang H, Yan Q & Yu W, 2.5 D modelling of wave propagation in longitudinally curved viscoelastic structure using a coupled FEM-PML approach. *Eng Struct*, 226 (2021) 111337.

15 Dash JN, Das R & Jha R, AZO coated microchannel incorporated PCF-based SPR sensor: a numerical analysis. *IEEE Photonics Technol Lett*, 30 (2018) 1032.

16 Jiang G, Fu Y & Huang Y, High birefringence rectangular-hole photonic crystal fiber. *Opt Fiber Technol*, 26 (2015) 163.

17 Razzak SMA, Namihira Y, Begum F, Kaijage S, Hai NH & Zou N, Design of a decagonal photonic crystal fiber for ultra-flattened chromatic dispersion. *IEICE Trans Electron*, 90 (2007) 2141.

18 Ried K, Eng P & Sali A, Screening for circulating tumour cells allows early detection of cancer and monitoring of treatment effectiveness: an observational study. *Asian Pac J Cancer Prev*, 18 (2017) 2275.

19 Ahmed K, Jabin MA & Paul BK, Surface plasmon resonance-based gold-coated biosensor for the detection of fuel adulteration. *J Comput Electron*, 19.1 (2020) 321.

20 Vial A, Grimault AS, Macías D, Barchiesi D & De La Chapelle ML, Improved analytical fit of gold dispersion: Application to the modeling of extinction spectra with a finite-difference time-domain method. *Phys Rev B*, 71 (2005) 085416.

21 Maier SA, Plasmonics: fundamentals and applications. *New York: springer*, (2007).

22 Jahan N, Rahman MM, Ahsan M, Based MA, Rana MM, Gurusamy S & Haider J, Photonic crystal fiber based biosensor for pseudomonas bacteria detection: A simulation study. *IEEE Access*, 9 (2021) 42206.

23 Sakib MN, Islam SR, Mahendiran TV, Abdulrazak LF, Islam MS, Mehedi IM, Kamrunnahar QM, Momtaj M, Hassan MW, Amiri IS & Hossain MB, Numerical study of circularly slotted highly sensitive plasmonic biosensor: a novel approach. *Results Phys*, 17 (2020) 103130.

24 Rakibul Islam M, Iftekher AN, Rakibul Hasan K, Nayen MJ & Bin Islam S, Dual-polarized highly sensitive surface-plasmon-resonance-based chemical and biomolecular sensor. *Appl Opt*, 59 (2020) 3296.

25 Liu W, Liu C, Wang J, Lv J, Lv Y, Yang L, An N, Yi Z, Liu Q, Hu C & Chu PK, Surface plasmon resonance sensor composed of microstructured optical fibers for monitoring of external and internal environments in biological and environmental sensing. *Results Phys*, 47 (2023) 106365.

26 Kriti B, Bhavana SJ & Renu K, Biofabrication and optimization of silver nanoparticles using *Campsis* sp. to explore their antimicrobial properties. *Indian J Biochem Biophys*, 59 (2022) 1176.

27 Geethalakshmi R, Sirajunnisa AR, Logeswari R & Renganathan S, Fabrication of phyco-functionalized zinc oxide nanoparticles and their *in vitro* evaluation against bacteria and cancer cell line. *Indian J Biochem Biophys*, 60 (2023) 770.

28 Ganjipour G, Heshmati M, Hashemi M & Entezari M, Administration of Curcumin, Betanin, and CoQ10 combined with nickel oxide, iron superoxide nanoparticles show preventive effects in breast cancer: Effect on apoptosis pathway and MiR-455 expression. *Indian J Biochem Biophys*, 60 (2023) 790.

29 Sonali, Rawat A & Yadav M, Nanotechnology in vaccine and immunology. *Indian J Biochem Biophys*, 59 (2022) 1135.

30 Sachin, Raj R, Dhiman S & Shakya L, Nanotechnological interventions in sustainable agriculture. *Indian J Biochem Biophys*, 59 (2022) 1153.

31 Trilaksana H, Thanmayalaxmi D & Suvitha A, ADMET, Pharmacokinetic and Docking properties of the fungal drug 2- (2, 4-difluorophenyl)-1, 3-bis (1, 2, 4-triazol-1-yl) propan-2-ol by using Quantum computational methods. *Indian J Biochem Biophys*, 60 (2023) 58.

32 Qian-wen W, Jae-sik J & Jae Kyung K, Effects of heavy metals on the viability of A549 cells. *Indian J Biochem Biophys*, 59 (2022) 726.